Author's manuscript (accepted version)

The original published version of the article can be find at:
European Journal of Physiology
ISSN 0031-6768
Volume 463 Number 6
Pflugers Arch - Eur J Physiol (2012) 463:829-844
DOI 10.1007/s00424-012-1103-1

http://www.springerlink.com/content/g141834546771572/
http://www.ncbi.nlm.nih.gov/pubmed/22547003

Activation of muscarinic receptors increases the activity of the granule neurones of the rat dorsal cochlear nucleus — a calcium imaging study

Áron Kőszeghy[1], János Vincze[1], Zoltán Rusznák[1,2], Yuhong Fu[2], George Paxinos[2,3], László Csernoch[1], Géza Szücs[1]

[1]University of Debrecen, Medical and Health Science Center, Department of Physiology, H-4012 Debrecen, Nagyerdei krt 98, Hungary

[2]Neuroscience Research Australia, Sydney, NSW, 2031, Australia

[3]The University of New South Wales, NSW 2052, Australia

Short title: Muscarinic modulation of the granule cells in the rat DCN

Send all correspondence to
Géza Szücs MD PhD
Department of Physiology, University of Debrecen, MHSC
H-4012 PO Box 22
E-mail: szucs.geza@med.unideb.hu
Phone: 0036-52-255575
Fax: 0036-52-255116

Abstract

Acetylcholine modulates the function of the cochlear nucleus via several pathways. In this study the effects of cholinergic stimulation were studied on the cytoplasmic Ca^{2+} concentration of granule neurones of the rat dorsal cochlear nucleus (DCN). Ca^{2+} transients were recorded in Oregon-Green-BAPTA 1-loaded brain slices using a calcium imaging technique. For the detection, identification, and characterisation of the Ca^{2+} transients, a wavelet analysis-based method was developed. Granule cells were identified on the basis of their size and localisation. The action potential-coupled character of the Ca^{2+} transients of the granule cells was established by recording fluorescence changes and electrical activity simultaneously. Application of the cholinergic agonist carbamyl-choline (CCh) significantly increased the frequency of the Ca^{2+} transients (from 0.37 to 6.31 min^{-1}, corresponding to a 17.1-fold increase; n = 89). This effect was antagonised by atropine, whereas CCh could still evoke an 8.3-fold increase of the frequency of the Ca^{2+} transients when hexamethonium was present. Using immunolabelling, the expression of both type 1 and type 3 muscarinic receptors (M1 and M3 receptors, respectively) was demonstrated in the granule cells. Application of 1,1-dimethyl-4-diphenylacetoxypiperidinium iodide (an M3-specific antagonist) prevented the onset of the CCh effect, whereas an M1-specific antagonist (pirenzepine) was less effective. We conclude that cholinergic stimulation increases the activity of granule cells, mainly by acting on their M3 receptors. The modulation of the firing activity of the granule cells, in turn, may modify the firing of projection neurones, and may adjust signal processing in the entire DCN.

Keywords Hearing – cholinergic modulation – immunolabelling – muscarinic receptor subtypes – pirenzepine – 1,1-dimethyl-4-diphenylacetoxypiperidinium iodide

Introduction

Acoustic information is carried to the projection cells of the dorsal cochlear nucleus (DCN) mainly directly, by axons belonging to the type I spiral ganglion neurones. These fibres make excitatory synaptic contacts with the basal dendritic trees of the pyramidal neurones as well as with some of the dendrites of the giant cells. Moreover, somatosensory information also reaches some of the projection neurones of the DCN, via an indirect 'somatosensory afferents-granule cell-parallel fibre' pathway.

Granule cells are the smallest and most numerous neurones of the DCN, with a somatic diameter of 6–8 μm [1, 22, 23]. Their axons travel towards the outer layers of the DCN, and eventually form the parallel fibre network which provides a major excitatory, glutamatergic input for the apical dendritic trees of the pyramidal cells, and for the superficially situated dendrites of the giant neurones ([20, 31, 40]; for a review see [25]). Granule cells, in turn, are contacted by axons carrying somatosensory information, mainly originating from the cuneate nucleus. Some of the granule cells are also contacted by acoustic fibres [19] and by axons arriving from higher acoustic centres [4, 31], hence they are often regarded as neurones that integrate acoustic and somatosensory information and modify the activity of projection neurones accordingly.

Although the majority of the fibres contacting the granule cells are glutamatergic [1, 31, 40], some of them (e.g., the cochlear mossy fibres) are thought to release acetylcholine (ACh), as indirectly inferred by the acetylcholinesterase positivity detected in the granule cell region [20, 31]. This observation raises the possibility that the activity of the granule cells may also be adjusted by cholinergic modulation. It has also been proposed in a recent study that the synaptic transmission occurring between the parallel fibres and the dendrites of the giant cells may also be modulated by presynaptic muscarinic receptors belonging to the M3 subtype [26].

Beyond the lines of evidence pointing towards the possible cholinergic modulation of the granule cells, several morphological and functional studies have demonstrated that ACh might be important in fine tuning the function of the cochlear nucleus (CN) in general [21]. For example, it has been shown that cholinergic axons originating from the trapezoid nucleus [33] and from the superior olivary complex [11] terminate in the CN, and vesicular choline acetyltransferase positive boutons have been described to contact various cell types of the CN [43]. Moreover, expression of muscarinic receptors has been demonstrated, along with their expression patterns, in the CN [41, 42]. As for the possible function of these inputs, extracellular recordings have

shown that cholinergic stimulation increases the firing frequency of both 'regularly firing' and 'bursting' neurones of the DCN — an effect that is predominantly mediated by muscarinic receptors [5]. Finally, 94% of the spontaneously active multiunit recording sites of the fusiform layer showed a change in their activity pattern when the cholinergic agonist carbamyl-choline (CCh) was applied [44].

Despite the apparent significance of the cholinergic modulation in the CN, and the findings indicating the involvement of the granule cells in this effect, no direct experimental evidence is available that can attribute changes in the functional properties of the granule neurones to cholinergic modulation. In the present study we report on the implementation of a calcium imaging technique for the detection and characterisation of Ca^{2+} transients evoked in granule cells situated in brain slices prepared from the rat DCN. Using this technique, we demonstrate an increase in the frequency of activity-related Ca^{2+} transients of the granule cells in response to cholinergic stimulation. Moreover, we provide evidence that this effect is chiefly mediated by M3 receptors expressed by the granule neurones.

Materials and methods

Animal care and preparation of the cochlear slices

The functional experiments were carried out on 8–10-day-old Wistar rats of both sexes. The details of the dissection method used in the imaging experiments were described earlier [26, 30]. In short, the animals were killed by decapitation, the brains were removed as quickly as possible, and they were transferred into ice-cold low-sodium artificial cerebrospinal fluid (LaCSF; see below). The brain was bisected along the midsagittal plane, the cerebral hemispheres and the cerebellum were removed, and the two halves of the brainstem were glued onto a metal block on their midsagittal surface. Parasagittal slices (thickness: 200 μm) were cut from the DCN using a Microm HM 650 V vibrotome (Microm International GmbH, Walldorf, Germany). The slices were transferred into an incubation chamber containing artificial cerebrospinal fluid (aCSF; see below), which was continuously bubbled with a mixture of 95% O_2 and 5% CO_2 at 37°C.

Solutions, chemicals and dye loading

The preparation was performed in LaCSF containing (in mM): sucrose, 250; $NaHCO_3$, 26; NaH_2PO_4, 1.25; glucose, 10; KCl, 2.5; ascorbic acid, 0.5; $CaCl_2$, 1; $MgCl_2$, 2. The imaging and loose-patch experiments were carried out in aCSF containing (in mM): NaCl, 125; KCl, 2.5; $NaHCO_3$, 26; glucose, 10; NaH_2PO_4, 1.25; $CaCl_2$, 2; $MgCl_2$, 1; myo-inositol, 3; ascorbic acid, 0.5; sodium pyruvate, 2. All chemicals were purchased from Sigma-Aldrich (St. Louis, MO, USA) unless noted otherwise.

For fluorescent calcium imaging, we used the acetoxymethylester form of the Oregon Green 488 BAPTA 1 fluorescent dye (OG488-AM; Invitrogen-Molecular Probes, Carlsbad, CA, USA). Stock solution (1 mM) was prepared by dissolving 50 μg OG488-AM in 40 μl dimethyl sulfoxide (DMSO) together with two detergents (0.5% pluronic acid and 0.1% cremophor EL), and stored in 4 μl aliquots at -20°C.

Ten minutes after their preparation, the slices were transferred into a Millicell CM culture plate insert (PICM01250; Millipore, Billerica, MA, USA) filled with aCSF. Following the transfer, the incubating solution was slowly replaced with 120 μl of the OG488-AM-containing loading solution, which was always freshly prepared by diluting one 4 μl aliquot of the stock solution with 116 μl aCSF, resulting in a final OG488-AM concentration of 33 μM. The Millicell insert containing the DCN slice and the loading

solution was then placed into one of the wells of a 24-well culturing plate, which was filled up with 450 µl aCSF previously. This manoeuvre resulted in the gradual reduction of the OG488-AM concentration inside the insert. The theoretical limit of this dilution was ~7 µM but neither the rate of the decrease in concentration nor the actual dye concentration was quantified. The 24-well plate, still containing the insert, was incubated (20–25 min) under tissue culture conditions (37°C, 5% CO_2) for dye-loading, and then the slices were transferred into an aCSF-filled chamber. An incubation period of 15–20 min at room temperature allowed the removal of the excess dye from the extracellular space as well as the hydrolysis of the intracellular OG488-AM.

In order to inhibit neurotransmission (i.e., to functionally 'uncouple' DCN neurones), the major chemical synaptic pathways were inhibited by applying a glutamatergic-glycinergic-GABAergic neurotransmission blocking cocktail (referred to as '3G cocktail' hereafter; [3]). The ionotropic glutamatergic receptors were inhibited by 10 µM 2,3-dihydroxy-6-nitro-7-sulfamoyl-benzo[f]quinoxaline-2,3-dione (NBQX) and 50 µM D-2-amino-5-phosphonopentanoate (D-AP5; Tocris Cookson Ltd., Bristol, UK); the glycinergic neurotransmission was blocked by using 1 µM strychnine, whereas GABAergic synapses were inhibited by 10 µM bicuculline. For cholinergic stimulation, CCh was applied extracellularly at concentrations of 5–100 µM. In some experiments, the effect of 100 µM ACh was also tested. To interfere with cholinergic stimulation mediated by muscarinic receptors, atropine was employed at a concentration of 50 µM. For the inhibition of the neural nicotinic cholinergic receptors, 100 µM hexamethonium was applied. When testing for the contribution of individual muscarinic receptor subtypes, either the M1 receptor-specific antagonist pirenzepine (Tocris) or the M3-specific 1,1-dimethyl-4-diphenylacetoxypiperidinium iodide (4-DAMP; Tocris) was used, both at a concentration of 1 µM. In some experiments 1 µM tetrodotoxin (TTX) was applied to prevent action potential firing. The significance of the external Ca^{2+} in producing Ca^{2+} transients was explored by applying nominally Ca^{2+}-free aCSF (in which $CaCl_2$ was replaced with equimolar amount of $MgCl_2$). In some experiments, the Ca^{2+}-free solution was supplemented with the L-type Ca^{2+} channel blocker nisoldipine (1 µM).

Intracellular calcium imaging

The DCN slices were viewed using a Zeiss Axioskop microscope (Carl Zeiss AG, Oberkochen, Germany) with a 20× or 63× water immersion objective. The microscope was equipped with a fluorescent imaging system (Till Photonics GmbH, Gräfelfing,

Germany) containing a xenon bulb-based Polychrome V light source, a CCD camera (SensiCam, PCO AG, Kelheim, Germany), an imaging control unit (ICU), and the Till Vision software (version 4.0.1.3). In the experiments monitoring Ca^{2+} concentration changes, the excitation wavelength was set to 488 nm by the monochromator of the Polychrome V light source. The fluorescent filter-set contained a dichroic mirror (Omega XF2031 505DRLPXR; Omega Drive, Brattleboro, VT, USA) and an emission filter (LP 515, Till Photonics). The parameters of the data acquisition were set by the Till Vision software. Throughout the calcium imaging, 8×8 binning of the 1.4 megapixel camera was employed (resulting in frames with 172×130 pixel resolution), the frame rate was set to 10 Hz.

For the precise determination of the somatic diameter of the granule cells, confocal microscopy was employed in a few cases. These measurements were carried out using a Zeiss LSM 7 Live confocal laser scanning microscope (Carl Zeiss AG). Several series of two-dimensional (x-y) images were recorded using a 20× objective (at 10 frames/s with a resolution of 512×512 pixels). The OG488 dye was excited with an argon ion laser at 488 nm. Z-stack images were also obtained using a 40× oil immersion objective. The thickness of the optical slices was 0.4 μm. Typically, 70 slices were obtained in one Z-stack. Cell diameters were determined from the reconstructed 3D images.

In the present work Ca^{2+}-related fluorescence intensity changes were recorded and analysed, but no attempts were made to calibrate the fluorescence values or to convert them to actual Ca^{2+} concentration. Nevertheless, for the sake of simplicity, the terms 'Ca^{2+} concentration' and 'Ca^{2+} transient' are used alternatively instead of the more precise 'fluorescence intensity' or 'fluorescence transient' expressions.

Extracellular loose-patch recording

For extracellular loose-patch recording of the neuronal action potential firing, micropipettes filled with aCSF were used (resistance ≈ 3–4 MΩ). The electrode was positioned in the close vicinity of the cell under visual control, using a PCS-6000 micromanipulator (EXFO-Burleigh, Mississauga, Ontario, Canada). During recordings, the tip of the microelectrode was in contact with the cell of interest with a seal resistance of ≥ 40 MΩ. The electrical activity of the cells was recorded in voltage-clamp mode using an Axopatch 200A amplifier (Molecular Devices, Union City, CA, USA). Data acquisition was performed at 10 kHz sampling rate with a 'gap-free' protocol using the Clampex 10.2 software (Molecular Devices). Off-line filtering and data

analysis of the loose-patch current recordings were performed using the Clampfit 10.2 program (Molecular Devices).

Analysis of the fluorescence intensity changes

For processing the Ca^{2+} imaging data, the recorded frames were exported into 16-bit TIF-movies that were viewed and analysed using the ImageJ software (National Institutes of Health). Data analysis started with manual selection of regions of interest (ROIs) whose shape, distribution, and size indicated that they corresponded to dye-loaded cell bodies. In the next step, the mean fluorescence intensity values of the ROIs were determined as a function of time, using the multi measure function of the ImageJ program. The resting fluorescence intensity of a given ROI was determined by averaging data points obtained during activity-free periods which were at least 25-cycle-long. All fluorescence data points were referred to the nearest preceding resting intensity value and presented in the figures in a percentage form. Although these plots are suitable for illustrating time-dependent fluorescence intensity changes, they are inconvenient for a manually performed quantitative analysis due to the plethora of activity-related fluorescence transients.

To process large quantities of data, a software capable of noise filtration, semi-automatic detection of the Ca^{2+} transients, and description of their kinetic features was developed. This software is the modification of a method applied earlier for the detection of elementary Ca^{2+} release events in skeletal muscle preparations [35, 38]. In short, a stationary wavelet transform on the fluorescence records was performed to decompose them into different frequency components. During this calculation the one-dimensional version of the transform was used. The algorithm is an implementation of the *á trous* stationary wavelet transform, using the B-spline of degree 3 as the scaling function. The convolution of the signal at a given step (F_i; at the first step it is the original signal, F_0) and the appropriately calibrated version of the scaling function was calculated, yielding a low-pass filtered signal (F_{i+1}). Subsequently, a high-pass filtered signal (W_{i+1}) was obtained as the difference between the newly calculated low-pass filtered signal and the signal obtained in the previous step ($F_{i+1} - F_i$). Because of the previous low-pass filtering, the high-pass filtered signals (W_i) had band-pass characteristics compared to the original signal. After n steps of the calculation, the original signal could be recalculated by applying the inverse transform $F_0 = F_n + \Sigma W_i$.

In order to improve the signal-to-noise ratio, and to facilitate event detection, a denoised signal (F_d) was calculated from the original records. Eventually, F_d was

obtained from the inverse transform during which the coefficients of the first two wavelet levels (W_1 and W_2) corresponding to high frequency noise were eliminated. It has to be noted, however, that denoising is a compromise, as this process, like every other type of noise filtration, alters the shape of the transients. To estimate the extent of this alteration, the frequency spectra of the original and the wavelet filtered fluorescence traces were compared using Fourier analysis. It was found that components having frequencies lower than 0.5 Hz were mostly preserved. However, at 0.51 Hz, 0.80 Hz, and 1.13 Hz, the removal of the discrete frequency components was 25%, 50%, and 75%, respectively. This observation indicates that the denoising protocol effectively reduces the high frequency noise, but preserves the frequency range that is suitable for the detection of the Ca^{2+} signals. For this detection, the first time derivative of F_d was calculated, and continuous sections of points with values above a pre-defined threshold (0.04 s^{-1}) were considered as transients. Each such section was extended to the nearest local minimum and maximum on the F_d trace (to get the rising phase of the transient), and then further extended to the next local minimum to get the whole transient.

Comparison of the original and the corresponding denoised traces indicated that the algorithm could not detect every Ca^{2+} event, and this was particularly evident in the case of high frequency activity. Such activity often resulted in (partially) fused Ca^{2+} transients, whose peaks were sometimes filtered out by the denoising protocol. Based on the comparison with the original traces, these fused transients were eliminated manually (as they were not suitable for kinetic analysis), even though this procedure resulted in an underestimation of the CCh-induced Ca^{2+} transient frequency increases. Further details of the software as well as the parameters used for the characterisation of the Ca^{2+} transients are given in Results.

Immunohistochemistry

Rats (aged 15 days and 1 month, n = 2 in either group) were euthanized with a lethal dose of sodium pentobarbitone (240 mg/kg body weight), and perfused through the left ventricle with 4% paraformaldehyde prepared in 0.1 M phosphate buffer (PB; pH = 7.4, 4°C). The brains were postfixed in the same fixative for 2 hours at 4°C, and cryoprotected in 30% sucrose-buffer overnight. Serial sections (both sagittal and coronal) were cut at 40 µm using a Leica CM 1950 cryostat (Leica Mycrosystems GmbH, Wetzlar, Germany). The sections containing the CN were consecutively harvested and immunohistochemically stained using M1-specific (1:200; raised in rabbit; Alomone Labs Ltd., Jerusalem, Israel) and M3-specific (1:200; raised in rabbit;

MBL International Corporation, Woburn, MA, USA) primary antibodies. The sections were blocked in 5% serum, incubated with either the M1- or the M3-specific antibody for 2 days at 4°C, and then incubated with goat anti-rabbit Alexa488 secondary antibody (1:250; Invitrogen, Mulgrave, VIC, Australia) for 2 hr at room temperature. Finally, the sections were washed, counterstained with 4′,6-diamidino-2-phenylindole (DAPI), dilactate (Invitrogen), mounted, and coverslipped with a fluorescence mounting medium (Dako, Campbellfield, VIC, Australia). The fluorescent images demonstrating the M1- and M3-labelling patterns of the CN were acquired with the 20× or 40× objective of a confocal microscope (Nikon Eclipse 90i; Nikon, Tokyo, Japan). For the visualisation of the Alexa Fluor 488 and DAPI signals, excitation wavelengths of 488 nm and 405 nm were employed in combination with 'B-2A' and 'DAPI' filter sets, respectively. Reconstruction of the composite images as well as the preparation of the final forms of the illustrations were performed using Adobe Photoshop CS5 (Adobe Systems Inc., San Jose, CA, USA). Occasionally, digital images were corrected for brightness and contrast, but in these instances the entire image was processed in the same way.

Statistics

For statistical analysis of the data, tests suitable for processing data sets showing non-normal distribution were used. When comparing averages obtained from independent populations, the Mann-Whitney test was applied. On comparing averages obtained from the same population, the Wilcoxon signed-rank test was used. Results are given as mean ± S.E.M.

Results

Characterisation of the Ca^{2+} transients recorded in DCN slices

On recording Ca^{2+}-related fluorescence intensity changes in the DCN slices, Ca^{2+} transients showing rather heterogeneous time courses were observed (Fig. 1a). The image shown in the left part of Fig. 1a demonstrates four ROIs, whose average fluorescence intensity changes were calculated and plotted as a function of time (right part of Fig. 1a). The ROIs (and traces) marked as neurone 1 and neurone 2 represent Ca^{2+} transients showing a repetitive character, with individual transients having rapid rising and slower falling phases. The rapid Ca^{2+} transients did not always occur as separate events; rather they showed (at least partial) fusion (as seen in the case of the first two transients marked with a box in the trace belonging to neurone 2). As opposed to the rapid transients, slowly developing and longer-lasting fluorescence intensity changes were also observed (as exemplified by traces marked as glia 1 and glia 2 in Fig. 1a).

To establish the possible origin of the rapid and slow transients, and to reveal the suspected interdependence of the Ca^{2+} transients and the membrane potential changes, simultaneous calcium imaging and extracellular loose-patch recording experiments were performed (Fig. 1b). On comparing the optical and electrical recordings, it was noted that the rapid Ca^{2+} transients were preceded by current signals (one of them is shown in the insert of Fig. 1b on an expanded time scale). The average duration of the current signals exemplified in Fig. 1b (0.75 ± 0.01 ms measured at 50% of the peak amplitude; $n = 87$) indicated that they corresponded to neuronal action potentials. Altogether 88 rapid Ca^{2+} events were examined under these experimental conditions, and 87 of these transients (98.9%) were preceded by action potentials. This strong correlation of the action potentials and rapid Ca^{2+} transients suggested that the rapid signals were neuronal Ca^{2+} transients developing as the consequence of the preceding action potential firing of the neurones.

The decisive role of action potentials in evoking the rapid Ca^{2+} transients was confirmed by applying TTX. Fig. 1c presents recording from a ROI that produced rapid Ca^{2+} transients. To facilitate action potential firing, the extracellular K^+ concentration was increased to 8 mM. As shown, the application of 1 μM TTX in the incubating medium prevented the genesis of the rapid transients. Altogether 4 active ROIs (in 2 slices prepared from 2 animals) were examined in the presence of TTX with the same

result. This observation not only is further evidence for the neuronal origin of the rapid transients, but also indicates that any modification of the rapid Ca^{2+} transients could be regarded as the consequence of the altered activity pattern of the neurones.

The interdependence of the action potentials and the rapid transients was further challenged by interfering with the Ca^{2+} entry through voltage-gated Ca^{2+} channels. In these experiments, the brain slices were incubated in nominally Ca^{2+}-free extracellular solution for 10–30 min (n = 3 in 2 slices from 2 animals). As the result, first marked attenuation of the rapid transients was experienced and then the transients disappeared along with the cessation of the firing activity of the cells (data not shown). In two other cells the Ca^{2+} withdrawal was combined with the application of 1 μM nisoldipine (an established blocker of the L-type Ca^{2+} channels). As Fig. 1d indicates, under these conditions the action potentials still persisted (although their frequency decreased), whereas rapid Ca^{2+} transients did not occur (n = 2 in 2 slices from the same rat), indicating that an action potential-dependent Ca^{2+} entry plays a decisive role in the generation of the rapid Ca^{2+} transients.

Fig. 1e presents the recording of the electrical activity of a cell producing slow Ca^{2+} transients. It is obvious that in this case the fluorescence transient is not related to action potential-like spikes. Altogether two ROIs were investigated (in 2 slices), and none of the slow Ca^{2+} transients (n = 15) was preceded by action potential firing. On the basis of this observation we conclude that the slow Ca^{2+} transients do not reflect neuronal activity, thus they are most likely produced by Ca^{2+} concentration changes occurring in non-neuronal cells (most likely astrocytes). Apart from characterising their kinetic features, the slow transients were not investigated further in the present study.

Quantitative analysis and classification of the Ca^{2+} transients

Generally, Ca^{2+} transients similar to those exemplified in Fig. 1 could be easily identified. Moreover, on the basis of their kinetic features, we could classify them as rapid or slow events by visual inspection only. In some cases, however, the detection and/or classification of the transients were far more difficult, necessitating the application of an objective technique. In addition, we also wanted to establish the basis of an automatic method that would allow reliable identification and analysis of a large number of rapid Ca^{2+} transients. This method would be a particularly useful alternative to study the activity of neuronal networks, since electrophysiological measurements on a large number of neurones are rather complicated to carry out. In the present work a ‘semi-automatic’ version of the analysis was applied, consisting of manual ROI

selection, manually verified event detection (see Materials and methods), and automatic classification of the Ca^{2+} transients into rapid (i.e., action potential-coupled) or slow (i.e., non-action potential-coupled) signals. The kinetic properties and other characteristics of the detected Ca^{2+} transients were also automatically determined.

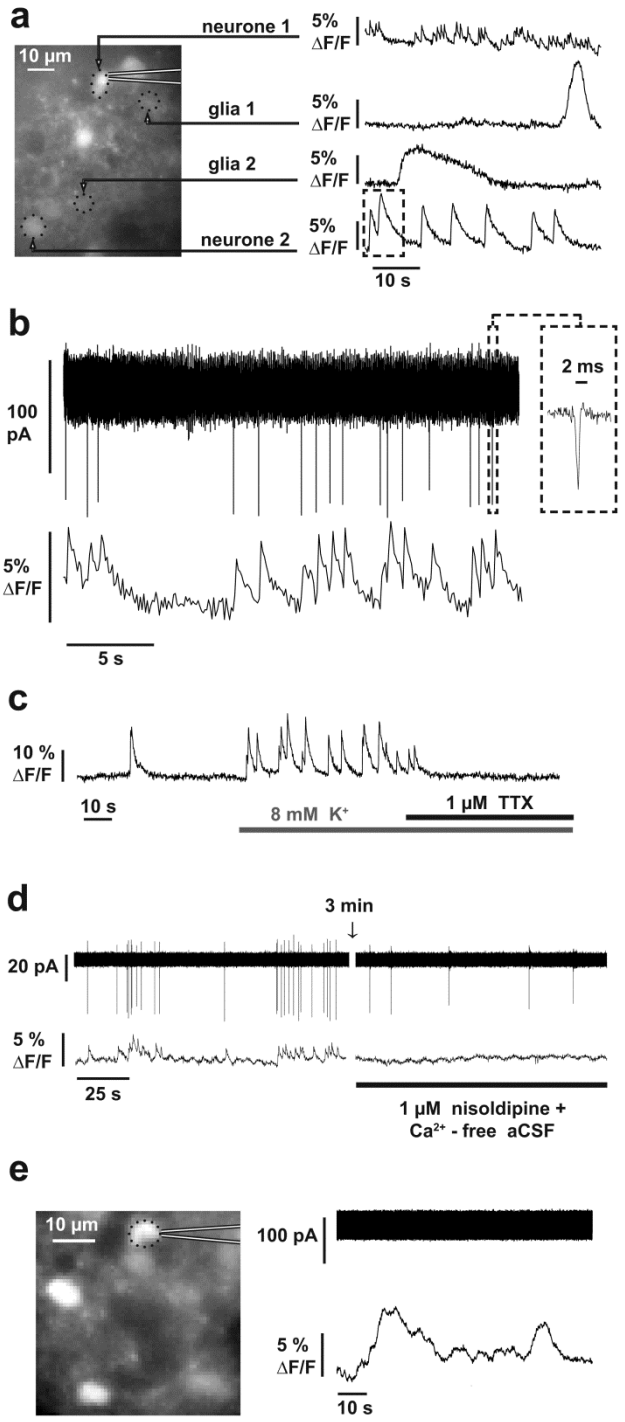

Figure 1: Intracellular Ca^{2+} transients and electrical activity of OG488-loaded DCN cells. **Panel a**: a high magnification (63×) wide-field fluorescence image (left part). Both the contours of the micropipette (digitally enhanced for visibility) used for loose-patch recording and the selected ROIs (dots forming circles) are indicated. The arrows marked with neurone 1 and neurone 2 indicate two neurones, while those marked with glia 1 and glia 2 show two non-neural (likely glial) cells. The right part of the panel presents fluorescence transients recorded from the cells shown on the left side and connected with the arrows. The box on the trace labelled as 'neurone 2' indicates two partially fused transients. **Panel b**: simultaneous current (upper trace) and fluorescence (lower trace) recording from a cell producing rapid transients (same as neurone 1 in panel a). The insert depicts a current transient on an expanded time scale. **Panel c**: fluorescence trace recorded from a cell in the presence of increased extracellular K^+ concentration, in the absence and in the presence of TTX (the incubation times are indicated by horizontal lines). **Panel d**: simultaneous current (upper trace) and fluorescence (lower trace) recording from a cell in aCSF (left) and 3 min after the application of Ca^{2+}-free aCSF containing 1 µM nisoldipine (right). **Panel e**: a high magnification (63×) wide-field fluorescence image (left part). Both the contours of the micropipette and the selected ROI are indicated. The simultaneously recorded current and fluorescence traces shown in the right part of the panel were taken from the cell marked in the image on the left side. Note that the current calibration is different from that of panel b.

Fig. 2a compares the time course of a recorded, not processed ('raw') fluorescence trace (F) and its denoised derivative (F_d). In the course of the analysis, the program calculated nine parameters characterising each visually confirmed, solitary F_d transient. Seven of these parameters are commonly used in signal analysis, including the maximum amplitude of the transient (AMP); maximum speed of the rising phase; time to peak (TTP); integral; relaxation times to 20%, 50%, and 80% of the amplitude (RT20, RT50, and RT80, respectively). As indicated in 'Materials and methods', the wavelet transform-based noise filtration tended to misshape the onset of all rapid transients (see Fig. 2a, upper part). The term 'TTP', consequently, is used here only as a parameter characterising the F_d transients, and our TTP values cannot be directly compared with those provided in earlier reports for the description of the time course of Ca^{2+}-related fluorescence signals.

Besides the above, generally used parameters, two more parameters were also determined. 'd2-swing' is the difference between the maximum and minimum values of the second time derivative of F_d (d^2F_d/dt^2, denoted as d2 hereon) within the limits of a transient — the latter values represent the maximum positive and negative accelerations belonging to a Ca^{2+} transient (Fig. 2a, lower part). 'Discriminator' (D) was calculated as the ratio of d2-swing and AMP.

In order to differentiate between rapid and slow Ca^{2+} transients, a two-layer feed-forward artificial neural network (ANN) was 'trained' in MATLAB (The MathWorks Inc., Natick, MA, USA). ANN took all parameters characterising each Ca^{2+} transient as input, and calculated the probability of having rapid character for a given transient as output. Such ANNs are useful tools for the separation of sets based on certain criteria [39]. The training of the ANN is effectively a non-independent fine tuning of the separation thresholds of all nine parameters. For the present training, 74 rapid Ca^{2+} transients (whose action potential-coupled origin had not been confirmed), and 55 slow Ca^{2+} transients were chosen. For validation, Ca^{2+} transients were measured simultaneously with loose-patch recording [i.e., their action potential-coupled origin had been confirmed (n = 87) or rejected (n = 15)], and the trained ANN classified all transients correctly. All Ca^{2+} transients recorded during the pharmacological experiments of the present study (except for those investigating the simultaneous actions of the M1 and M3 receptor-specific antagonists) were tested with the trained and validated ANN, and 1518 out of the 1570 transients (96.7%) were classified as rapid (action potential-coupled) ones.

Figs 2b–2c illustrate the mean values of some parameters determined for all rapid (n = 1679) and slow transients (n = 70). The rapid Ca^{2+} transients had faster rising phase, which is reflected by significantly smaller TTP values (Fig. 2b). The RT80 values of the two populations of the transients were also statistically different, indicating that the slow transients lasted longer than the rapid ones (Fig. 2b). Moreover, the Discriminator parameter values of the two groups were also statistically different (Fig. 2c). The usefulness of the Discriminator parameter is illustrated in Figs 2d–2f, which show the distribution of the individual transients in a plane determined by any two of TTP, RT80, and Discriminator. To help orientation, polygons were constructed by connecting the marginal points of the rapid and slow populations. The combination of the Discriminator parameter with either RT80 (Fig. 2d) or TTP (Fig. 2e) resulted in a fairly good separation of the two types of transients. When combining RT80 and TTP, however, a distinct overlap of the rapid and slow transients was noted (Fig. 2f).

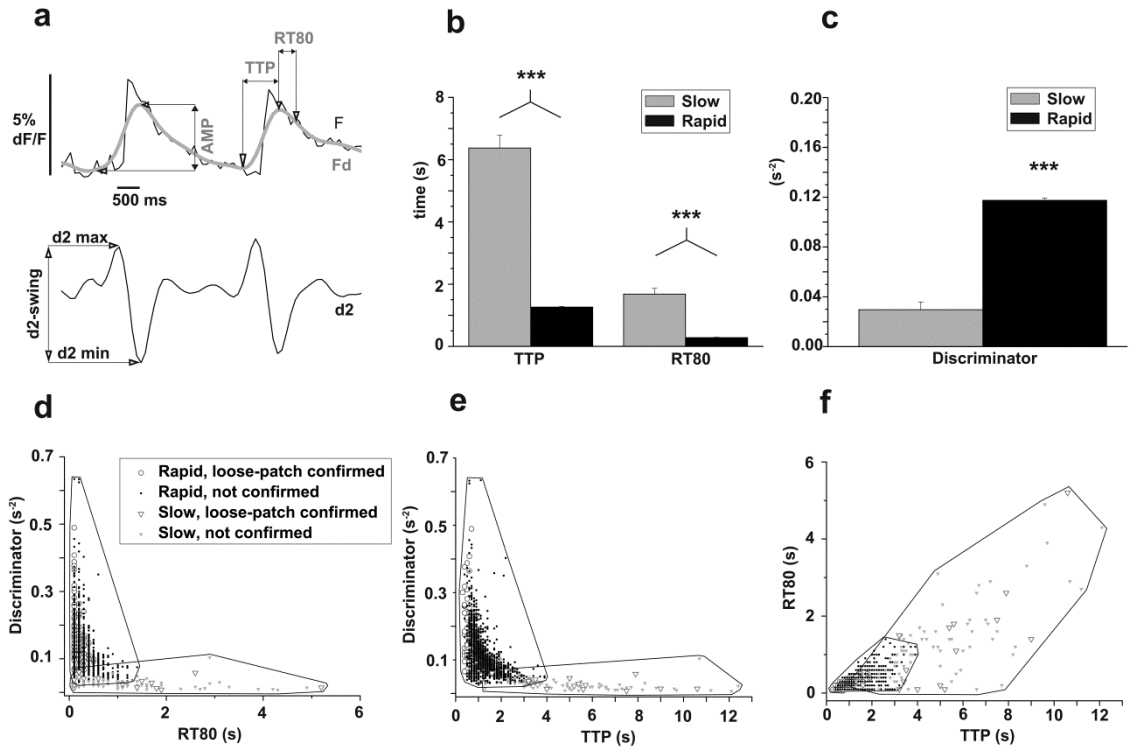

Figure 2: Parameters determined by the evaluation program. **Panel a**: raw (F, thin black line) and denoised (F_d, thick grey line) fluorescence traces (upper part), and the second time derivative of the F_d trace (d2, lower part). AMP: amplitude of the F_d transient; TTP: time to peak; RT80: relaxation time to 80% of the maximum. In the lower part, the determination of the d2-swing parameter is shown. **Panels b–c**: synopsis of some parameter values determined for all rapid (n = 1679) and slow transients (n = 70). Panel b compares TTP and RT80, while panel c presents the summary of the Discriminator values (see Results). ***: $p < 0.001$. **Panels d–f**: scatterplots of the RT80 and Discriminator (panel d), TTP and Discriminator (panel e) as well as TTP and RT80 (panel f). The polygons were created by connecting the marginal points of the corresponding data populations. In these panels the loose-patch confirmed and non-confirmed sub-populations of the transients were indicated with different symbols, but they were merged during the construction of the polygons.

Effects of CCh on the activity of the granule cells of the DCN

Having established the methodological details of the semi-automatic Ca^{2+} transient analysis, we could concentrate on the primary aim of the present work, and investigate the nature of the rapid, CCh-induced events in the DCN. Fluorescence imaging revealed that there were different cell types in the DCN slices. These cell types generated spontaneous Ca^{2+} transients that were somewhat variable in terms of their shape, onset, duration, etc. (see Fig. 1a). In the present work, however, we did not seek correlation between the cell types and their Ca^{2+} transients but focused on the investigation of the effects of cholinergic modulation on the activity of the granule neurones only. To achieve this, only those cells were considered which produced rapid Ca^{2+} transient(s) when CCh was applied, and whose cell body diameter was less than 8 μm. It should be noted that although these criteria ensured that other cell types of the DCN were excluded from the data analysis, this approach did not allow the estimation of the ratio of the CCh-sensitive cells within the entire granule cell population.

To illustrate the results of the cell selection procedure, Fig. 3a shows a bright field image of an OG488-loaded DCN slice with low (4×) magnification. Fig. 3b displays an epifluorescence image taken from the encircled area of Fig. 3a with higher (63×) magnification, where several dye-loaded neurones can be seen. On the basis of their size, localisation, and the morphology of the thin, non-branching process, the investigated cells were identified as granule neurones of the DCN. To support the validity of the method used for the determination of the diameter of the granule cells, in some experiments confocal microscopy was employed. Fig 3c shows a low magnification confocal image of a DCN slice, while Fig. 3d presents a high magnification image of the area indicated with the rectangle in Fig. 3c. The average diameter of granule cells identified in the confocal images was 7.5 ± 0.4 μm ($n = 9$).

Similarly to our previous works, the effects of cholinergic stimulation on the Ca^{2+} transients of the granule neurones were tested by a single extracellular application of the cholinergic agonist CCh. At the beginning of the measurements, however, the ACh sensitivity of the cells was tested in 2 slices prepared from 2 rats. In the presence of the 3G cocktail, the frequency of the transients was 0.22 ± 0.22 min^{-1}. In the presence of 100 μM ACh, an increase to 8.98 ± 1.52 min^{-1} was seen ($n = 6$, $p < 0.05$).

During the experiments investigating the effects of CCh, first aCSF supplemented with the neurotransmission blocking 3G cocktail was applied then CCh

was given in the continuous presence of the 3G cocktail. The frequency of the rapid Ca^{2+} transients occurring during the 3G incubation period (45–90 s) was regarded as control. The concentration-dependence of the CCh-induced activity of the granule cells was tested by applying increasing CCh concentrations in a cumulative manner. Fig. 3e gives the percentage of the granule neurones that started to respond to the cholinergic stimulation at the individual CCh concentrations (altogether 24 neurones were observed from 3 slices prepared from 3 rats). It can be seen that the majority of the cells increased their activity in the presence of 20 μM CCh, although additional cells started to respond at 50 and 100 μM. To ensure that all CCh-sensitive cells are activated, a saturating concentration of CCh was applied in all further experiments (100 μM for 90–120 s; Fig. 3f). Under the influence of the cholinergic agonist, an increase of the frequency of the rapid Ca^{2+} transients was observed in 89 granule neurones (situated in 33 DCN slices prepared from 19 rats). The average somatic diameter of these cells was 7.2 ± 0.1 μm. Considering all cells, CCh evoked a significant increase of the frequency of the Ca^{2+} transients (from 0.37 ± 0.11 min^{-1} to 6.31 ± 0.43 min^{-1}; $p < 0.001$; Fig. 3g).

As noted before, in the case of high-frequency firing, the rapid Ca^{2+} transients tended to fuse — resulting in an underestimation of their frequency. To approximate the level of this underestimation, the effects of 100 μM CCh were evaluated in experiments recording electrical activity and fluorescence transients simultaneously (in 5 slices from 4 animals). A representative recording from this set of the experiments is shown in Supplementary Fig. 1 together with the synopsis of the results. In short, after applying the CCh, the frequency of both the action potentials and the rapid Ca^{2+} transients increased significantly but this change was more substantial in the cases of the action potentials.

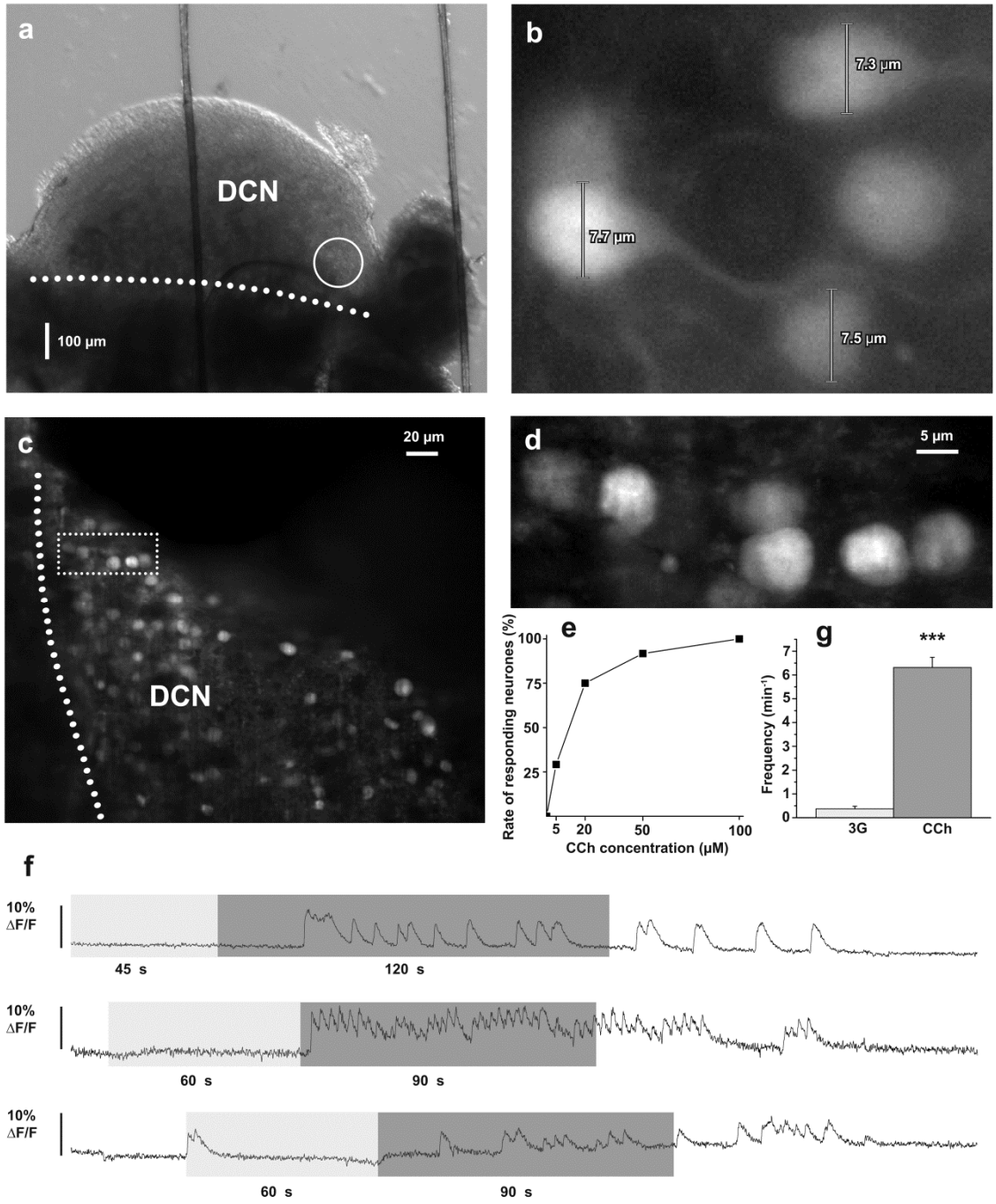

Figure 3: Effects of CCh on the Ca^{2+} transients of the granule neurones in the DCN. **Panels a–b**: localisation of OG488-AM-loaded granule neurones within the DCN as seen with low (4×; panel a) and high (63×; panel b) magnification. In panel a, the circle indicates the area from which the image of panel b was taken; dotted line marks the border between DCN and VCN. In panel b, the lines and numbers indicate the diameters of the somata. **Panels c–d:** confocal view of granule neurones in the DCN. Panel c presents a low magnification image (obtained with a 20× objective) taken from the dorsal surface of a DCN slice (dotted line indicates the border between the DCN and VCN). Panel d shows the area indicated with dotted rectangle in panel c at higher magnification (40× oil immersion objective). This panel was reconstructed as a maximum intensity projection of the Z-stack images. **Panel e**: percentage number of granule neurones that started to respond to CCh at increasing concentrations of the agonist. Altogether 24 neurones (= 100%) were observed in 3 DCN slices prepared from 3 rats. **Panel f**: representative Ca^{2+}-related fluorescence recordings taken from three ROIs from three different slices. Light grey background indicates the application of the 3G cocktail, while the dark grey background shows the application of 100 µM CCh in the continuous presence of the 3G cocktail. **Panel g**: synopsis of all experiments carried out in the same way as shown in panel f. The columns give the mean frequencies of the rapid Ca^{2+} transients before (light grey column) and during (dark grey column) the CCh treatment ($n = 89$; ***: $p < 0.001$).

In order to identify the receptors responsible for mediating the CCh effect, various cholinergic antagonists were needed. As these pharmacological experiments required repetitive application of CCh, it was necessary to check the consistency of the CCh-response, i.e., to answer the question whether the frequency in responding cells differs during two consecutive CCh challenges. Figs 4a–4b depict a granule neurone in which both the first (Fig. 4a) and the second CCh applications (Fig. 4b) evoked an increase in the firing activity, while Fig.4c presents the synopsis of all similar experiments. In 10 granule cells (accommodated by 5 slices prepared from 2 animals) 100 μM CCh significantly increased the frequency of the rapid transients (from 0.67± 0.38 min^{-1} to 5.00± 1.11 min^{-1}). After a recovery period of 8–10 min, the CCh application was repeated. During this second cholinergic CCh stimulation the firing frequency increased significantly as well (from 0.07 ± 0.06 min^{-1} to 2.74± 0.67 min^{-1}). Nevertheless, it is evident that the CCh-sensitivity of the neurones decreased between the two CCh-treatments — a phenomenon referred to as tachyphylaxis hereafter.

The next experiment tested whether the CCh-induced increase of the Ca^{2+} transient frequency is attenuated by the application of the general muscarinic receptor antagonist atropine. In these experiments (17 cells in 4 slices from 2 animals) first 100 μM CCh was added (in the presence of the 3G cocktail), which evoked the expected increase in the frequency of the Ca^{2+} signals (Fig. 4d). After washing out the CCh (8–10 min), 50 μM atropine was added to the incubating solution (still containing the 3G cocktail), then CCh was applied again (in the continuous presence of the 3G cocktail and atropine; Fig. 4e). The synopsis of these data is presented in Fig. 4f. As shown, the frequency of the Ca^{2+} transients significantly increased when CCh was applied (from 0.67 ± 0.41 min^{-1} to 7.39 ± 1.22 min^{-1}; n = 17). In contrast, when atropine was also present in the extracellular solution, the frequency of the Ca^{2+} transients did not change significantly. When the frequency of the CCh-induced rapid transients developing in the presence of atropine (Fig. 4f) was compared to those recorded during the second application of CCh (as described in conjunction with the tachyphylaxis experiments; Fig. 4c), a significant difference ($p < 0.01$) was observed, underscoring that atropine decreased the frequency of the transients far more effectively than did tachyphylaxis alone. This finding indicated that muscarinic receptors are involved in the mediation of the CCh effect on the granule cells.

In the next phase of the work, the possible roles of nicotinic receptors were tested using hexamethonium. In these experiments (15 cells situated in 6 slices prepared from 2 animals) 100 μM CCh was added to the extracellular solution (in the presence of

the 3G cocktail; Fig. 4g). Following a wash out period (8-10 min), 100 µM hexamethonium was added, and then CCh was applied again in the continuous presence of the 3G cocktail and hexamethonium (Fig. 4h). The summary of the results is presented in Fig. 4i. As shown, during the first CCh challenge, the frequency of the Ca^{2+} transients significantly increased (from 0.18 ± 0.14 min^{-1} to 7.54 ± 0.81 min^{-1}, n =15). When hexamethonium and CCh were present simultaneously, the frequency of the Ca^{2+} transients increased significantly as well (from 0.53 ± 0.4 min^{-1} to 4.40 ± 1.20 min^{-1}). No significant difference was found when the frequency of the rapid transients developing in the combined presence of CCh and hexamethonium (Fig. 4i) was compared to that recorded during the second CCh application of the tachyphylaxis experiments (Fig. 4c). This observation indicated that, as opposed to atropine, hexamethonium had the same effect as tachyphylaxis alone, emphasising that nicotinic cholinergic receptors do not have decisive roles in mediating the effects of CCh in the present set of experiments.

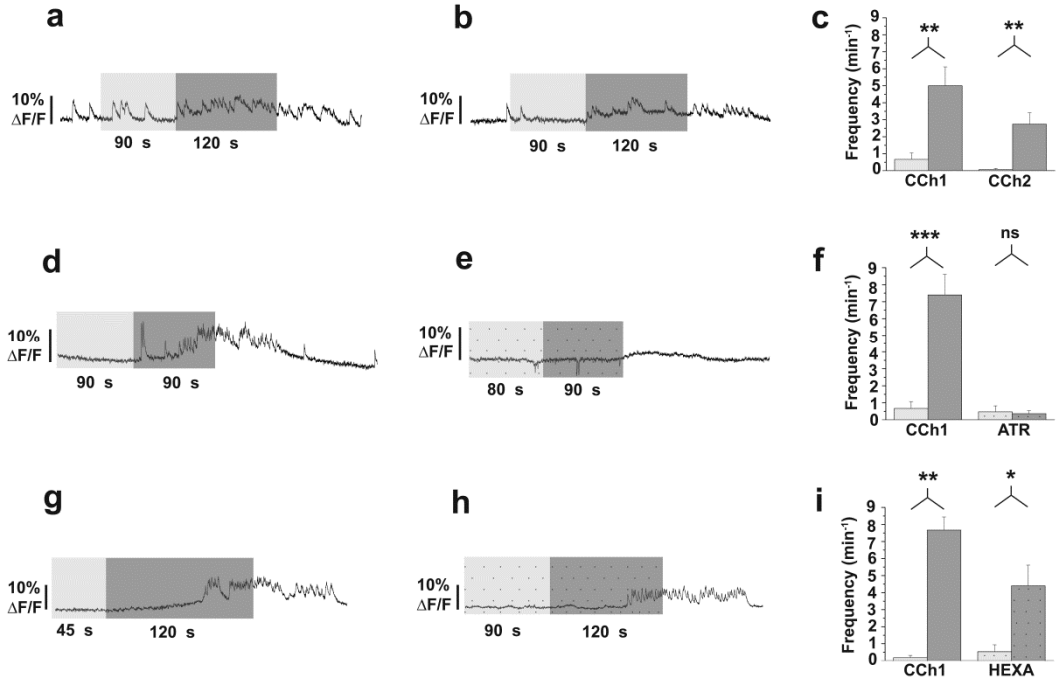

Figure 4: Effects of atropine and hexamethonium on the CCh-evoked Ca^{2+} transients of the granule neurones in the DCN. **Panels a–b**: activity of a granule cell in the presence of 3G cocktail (light grey background), and in the presence of 100 µM CCh (dark grey background) during the first (panel a) and second CCh application (panel b). **Panel c**: synopsis of all experiments where the repeated application of CCh was studied. The columns give the average frequency of the rapid transients during the 3G cocktail, in the absence (light grey columns) and in the presence of 100 µM CCh (dark grey columns) during the first (CCh1) and second (CCh2) CCh treatment (n = 10). **Panel d**: activity of a granule cell during the 3G cocktail (light grey background), and in the presence of 100 µM CCh (dark grey background). **Panel e**:

activity of the same granule cell as in panel d during the 3G cocktail containing 50 μM atropine (light grey background with dots), and in the combined presence of 50 μM atropine and 100 μM CCh (dark grey background with dots). **Panel f**: synopsis of all experiments where the effect of atropine on CCh-induced Ca^{2+} transients was studied. The columns give the average frequency in 3G cocktail in the absence (light grey columns) and in the presence of 100 μM CCh (dark grey columns) under control conditions (CCh1), and in the presence of atropine (ATR; n = 17). **Panel g**: activity of a granule cell during the 3G cocktail incubation (light grey background), and in the presence of 100 μM CCh (dark grey background). **Panel h**: activity of the same granule cell as in panel g during the 3G cocktail containing 100 μM hexamethonium (light grey background with dots), and in the combined presence of 100 μM hexamethonium and 100 μM CCh (dark grey background with dots). **Panel i**: synopsis of all experiments where the effect of hexamethonium on CCh-induced Ca^{2+} transients was studied. The columns indicate the average frequencies during the 3G cocktail in the absence (light grey columns) and in the presence of 100 μM CCh (dark grey columns) under control conditions (CCh1), and in the presence of hexamethonium (HEXA; n = 15). ns: nonsignificant; *: $p < 0.05$; **: = $p < 0.01$; ***: $p < 0.001$.

The role of M1 and M3 receptors in the CCh effects

The results presented so far indicated that i) the application of a cholinergic agonist increased the activity of the granule cells, and ii) mainly muscarinic receptors were involved in the mediation of the effect, with only limited — if any — contribution from the nicotinic ones. Since it was evident that activation of the muscarinic receptors resulted in an increase of the frequency of the intracellular Ca^{2+} transients, it was hypothesized that the possible receptors mediating this response were the M1, M3, and M5 subtypes, those members of the muscarinic receptor family that are known to be intimately coupled to the Ca^{2+} signalization pathway [8]. However, in one of our previous studies [26] we have demonstrated that in the time interval investigated in the present work (8–10 days postnatal) the amount of M5 receptor-specific mRNA hardly exceeded detection level, thus the potential role of this receptor subtype could be ruled out. As for the other two candidates, both M1- and M3-specific mRNA could be detected in the samples prepared from the entire CN, although the quantity of the M3-specific mRNA was some 4× greater than that of the M1-specific one. These observations suggested that the cholinergic effects observed in the present study were mediated by the M3 and/or M1 receptors. To investigate this hypothesis, M1 and M3 receptor-specific immunohistochemistry was employed in combination with confocal microscopy. For these experiments, two age groups were used: 15-day-old rats representing the level of maturation encountered in the functional experiments, and 30-day-old ones which corresponded to a more developed state. Comparison of the immunolabelling patterns did not reveal any apparent difference between these age groups. For this reason, the immunohistochemistry results obtained from the 30-day-old rats are demonstrated here (Fig. 5), whereas the immunolabelling pattern observed in the younger group is presented in Supplementary Fig. 2.

Both the anterior and posterior parts of the ventral CN (aVCN and pVCN, respectively) featured cells presenting strong immunopositivity for both M1 (Fig. 5a) and M3 (Fig. 5d) receptors. In addition, large cells showing prominent M1 expression were visible in the DCN. Although the M3 receptor-specific immunolabelling of these cells was somewhat weaker, large, positively labelled cells were also visible; especially in the deeper parts of the DCN (Fig. 5d, near the dotted line separating the DCN and VCN). Detailed description of the M1- and M3-specific labelling patterns of the CN was outside the scope of the present work.

To answer the question whether granule cells of the CN express either type of muscarinic receptors, specific attention was given to the area where granule cells are most easily found: the granule cell 'belt' separating VCN from DCN. This region (part of which is indicated by '*' in Figs 5b and 5e; see also Supplementary Fig. 2) could be easily identified on the basis of its localization. Moreover, the high density of the characteristic, small-sized, and densely packed granule cell nuclei was a reliable guide. As the immunolabelling revealed, the granule cells of the CN expressed M1 receptors (Figs 5c1–c3). The labelling appeared to be particularly intense in the surface membrane, and in some instances it showed a clearly patchy or grainy distribution (e.g., see the cell shown with arrow in Figs 5c1–c3), which may have indicated receptor aggregation at certain points of the cell surface membrane. As for the expression of the M3 receptor protein, the positivity of the granule cells was also obvious (Figs 5f1–f3), and the grainy appearance of the immunopositivity was even more pronounced than in the case of the M1 receptors. Moreover, it was also evident that not all cells in the granule cell area expressed M3 receptors. An example is presented in Figs 5f1–f3, where the cell indicated by '○' showed markedly different nuclear morphology (narrow, elongated nucleus as opposed to the more spherical ones characteristic of the granule cells) and did not present M3-specific immunopositivity. Although the precise identity of this and similar cells was not sought in the present work, they may have corresponded to representatives of a subclass of astrocytes that do not express M3 receptors [27]. Nevertheless, the existence of M3 receptor negative cells was an important observation, as it indicated that the immunohistochemistry results were not the consequences of non-specific labelling.

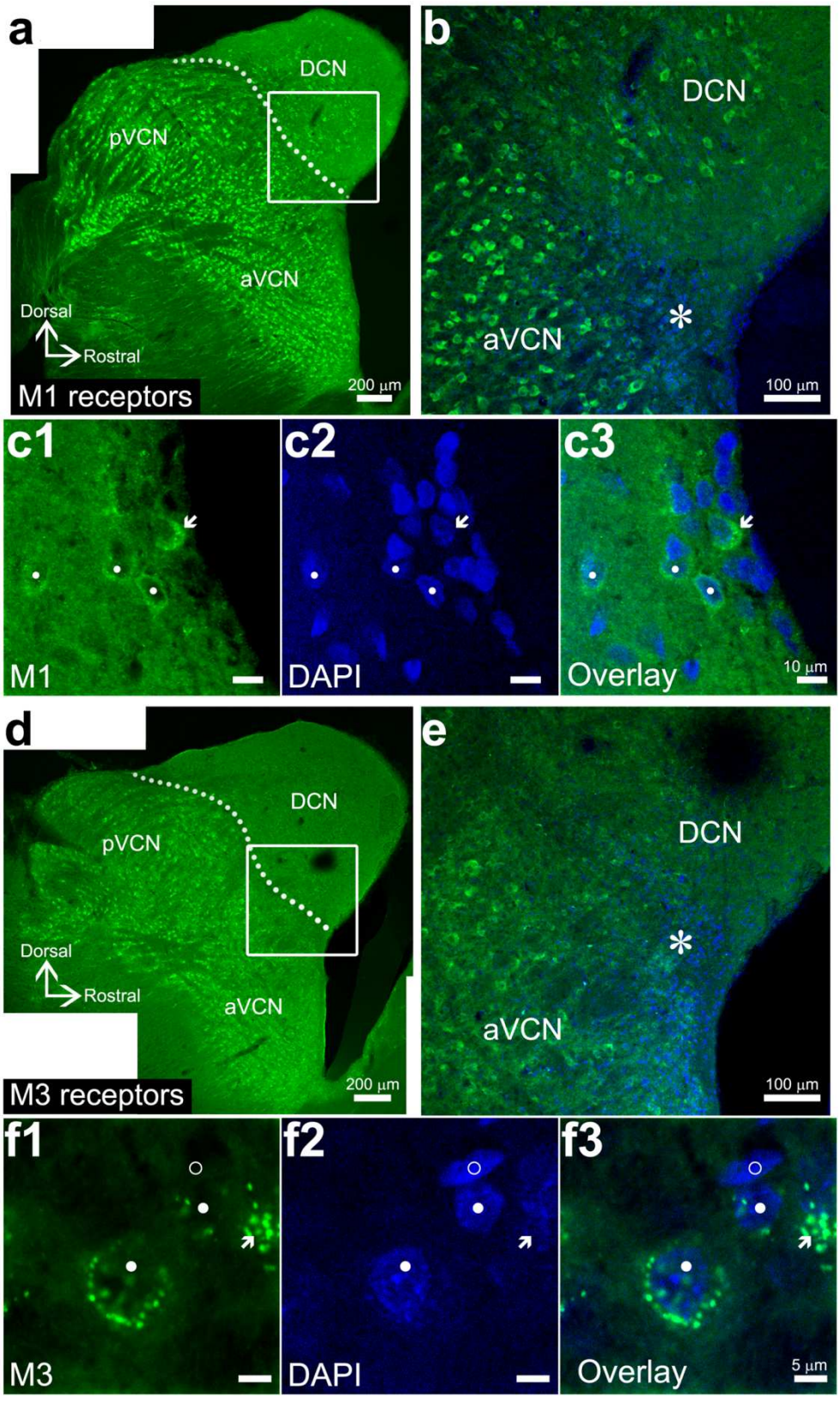

Figure 5: M1 and M3 receptor-specific immunolabelling in the rat cochlear nucleus. **Panel a**: composite image demonstrating a low magnification overview of the M1 receptor-specific immunolabelling pattern. The dotted line indicates the border between the dorsal and ventral parts of the nucleus; the white rectangle indicates the area which is shown in panel b. DCN, aVCN, and pVCN stand for dorsal cochlear nucleus, antero-ventral cochlear nucleus, and postero-ventral cochlear nucleus, respectively. **Panel b**: higher magnification view of the anterior margin of the cochlear nucleus. Star (*)

indicates part of the granule cell layer separating the dorsal and ventral parts of the nucleus. Note the high density of the small, DAPI-labelled nuclei (blue signal) in the indicated region. **Panels c1–c3**: high magnification images depicting the M1-specific labelling pattern of the granule cell region. Panel c1: M1-specific immunopositivity (green), panel c2: DAPI labeling (blue), panel c3: overlay image. White dots mark some of the granule cells demonstrating strong M1-specific immunopositivites. Note the cell marked with arrow where the grainy distribution of the immunoreactivity is particularly evident. **Panel d**: composite image demonstrating low magnification overview of the M3 receptor-specific immunolabelling pattern. Dotted line marks the border between the dorsal and ventral parts of the nucleus; white rectangle indicates the area which is shown in panel e. **Panel e**: higher magnification view of the anterior margin of the cochlear nucleus. Star (*) indicates part of the granule cell layer separating the dorsal and ventral parts of the nucleus. **Panels f1–f3**: high magnification images depicting examples of strongly M3 positive granule cells (white dots; panel f1: M3-specific immunopositivity, panel f2: DAPI labelling, panel f3: overlay image). The distinctly grainy appearance of the immunolabelling is evident in all instances. In the case of the cell marked with arrow, immunopositive granules situated on the top surface of the cell are visualised. Note the cell indicated by a circle (□) that presents distinctly different morphology of the cell nucleus (elongated rather than spherical) and demonstrates no M3 immunopositivity.

The results of the M1- and M3-specific immunolabelling experiments show that the granule cells of the CN express both types of receptors in either age group investigated. To reveal the functional significance of these receptor subtypes, Ca^{2+} imaging experiments were undertaken, using M1 (pirenzepine) and M3 receptor-specific (4-DAMP) muscarinic receptor antagonists. When testing for the significance of the M1 receptors (12 cells, accommodated by 4 slices prepared from 3 animals), first 100 μM CCh was added, which evoked the expected increase of the frequency of the Ca^{2+} transients (Fig. 6a). After washing out CCh (8–10 min), 1 μM pirenzepine was added to the incubating solution, and then CCh was applied again along with pirenzepine (Fig. 6b). The summary of these experiments is presented in Fig. 6c. As shown, in the presence of CCh, the frequency of the Ca^{2+} transients significantly increased (from 0.33 ± 0.17 min^{-1} to 6.72 ± 1.44 min^{-1}, $n = 12$). When pirenzepine was also present in the extracellular solution, the average frequency of the Ca^{2+} transients still increased significantly on CCh challenge (from 0.22 ± 0.10 min^{-1} to 3.29 ± 1.02 min^{-1}). Apparently, the attenuation of the frequency increase that was noted in the presence of pirenzepine did not differ statistically from the effect of tachyphylaxis (compare Figs. 4c and 6c), indicating that although M1 receptors are expressed by the granule cells, their functional significance in mediating cholinergic modulation is rather limited.

In the experiments aimed at the investigation of possible role of M3 receptors (studied in 15 cells situated in 5 slices prepared from 3 animals), a similar protocol was applied. First 100 μM CCh was applied alone (Fig. 6d), followed by a wash out period. In the next step, 1 μM 4-DAMP was applied, and then CCh was added again in combination with 4-DAMP (Fig. 6e). The synopsis of these experiments is presented in Fig. 6f. As shown, CCh significantly increased the frequency of the Ca^{2+} transients

(from 0.09 ± 0.06 min^{-1} to 5.93 ± 0.91 min^{-1}, n = 15). Finally, when 4-DAMP was also present, the frequency of the Ca^{2+} transients remained effectively the same on CCh application (0.40 ± 0.21 min^{-1} in control solution, 0.57 ± 0.25 min^{-1} in the combined presence of CCh and 4-DAMP). Moreover, if the frequency of the rapid transients seen in the combined presence of CCh and 4-DAMP (Fig. 6e) is compared to the frequency documented during the tachyphylaxis experiments (Fig. 4c), a significant difference ($p < 0.01$) can be noted, indicating that the cholinergic stimulation of the granule cells is mediated by M3 receptors.

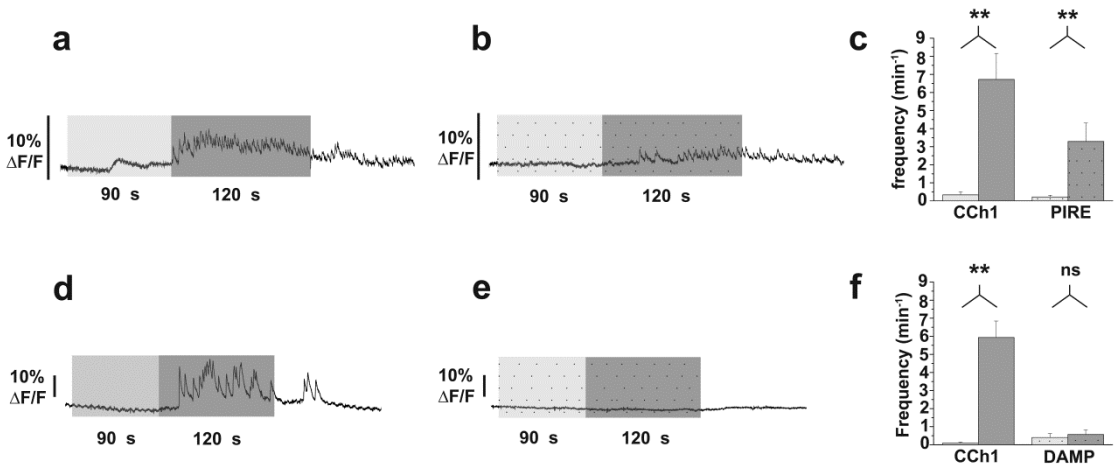

Figure 6: Effects of subtype-specific M-receptor antagonists on the CCh-evoked Ca^{2+} transients of the granule neurones in the DCN. **Panel a**: activity of a granule cell during the 3G cocktail (light grey background), and in the presence of 100 µM CCh (dark grey background). **Panel b**: activity of the same granule cell during the 3G cocktail containing 1 µM pirenzepine (light grey background with dots), and in the combined presence of 1 µM pirenzepine and 100 µM CCh (dark grey background with dots). **Panel c**: synopsis of all experiments where the effect of pirenzepine on CCh-induced Ca^{2+} transients was studied. The columns give the average frequency during the 3G cocktail in the absence (light grey columns), and in the presence of 100 µM CCh (dark grey columns) under control conditions (CCh1) and in the presence of pirenzepine (PIRE; n = 12). **Panel d**: activity of a granule cell during the 3G cocktail (light grey background), and in the presence of 100 µM CCh (dark grey background). **Panel e**: activity of the same granule cell during the 3G cocktail containing 1 µM 4-DAMP (light grey background with dots), and in the combined presence of 1 µM 4-DAMP and 100 µM CCh (dark grey background with dots). **Panel f**: synopsis of all experiments where the effect of 4-DAMP on CCh-induced Ca^{2+} transients was studied. The columns give the average frequencies during the 3G cocktail in the absence (light grey columns) and in the presence of 100 µM CCh (dark grey columns) under control conditions (CCh1) and in the presence of 4-DAMP (DAMP; n = 15). ns: nonsignificant; **: $p < 0.01$.

In order to investigate the consequences of blocking both M1 and M3 receptors simultaneously, combined application of 1 µM pirenzepine and 1 µM 4-DAMP was also tested (in 3 slices prepared from 3 animals). Before the application of the antagonists, 100 µM CCh significantly increased the frequency of the Ca^{2+} transients (from 1.11 ± 0.70 min^{-1} to 12.14 ± 2.76 min^{-1}, n = 9; $p < 0.01$). When the effects of the blockers were studied, the frequency of the Ca^{2+} transients was 0.44 ± 0.44 min^{-1} in the control solution and 0.78 ± 0.49 min^{-1} in the combined presence of CCh, pirenzepine, and 4-DAMP (the difference is not statistically significant). In contrast, when the

frequency of the rapid transients seen in the combined presence of CCh and both antagonists is compared to the frequency established in the tachyphylaxis experiments (Fig. 4c), a significant difference ($p < 0.05$) can be noted. These findings indicate that simultaneous inhibition of the M1 and M3 receptors has the same effect as the application of atropine or 4-DAMP alone.

Discussion

In this work calcium-related fluorescence transients produced by cells of the rat DCN were recorded. Moreover, a wavelet analysis-based technique was developed to identify these Ca^{2+} transients and to characterise their kinetic features. Specific attention was given to the rapid Ca^{2+} transients of the granule cells. These transients were preceded by action potentials and their frequency was significantly increased by cholinergic stimulation. The functional experiments indicate a decisive role of M3 receptors in generating CCh-induced Ca^{2+} transients, although M1 receptors were also detected by immunohistochemistry.

Calcium imaging in DCN brain slices

In the present work spontaneous and CCh-induced cytoplasmic Ca^{2+} concentration changes were monitored in cells situated in a DCN thin-slice preparation loaded with a fluorescent, Ca^{2+}-sensitive dye. The advantage of this technique is that large populations of neurones can be loaded with the preferred calcium indicator allowing the investigation of a large number of neurones simultaneously ([15, 32]; for review of techniques see [10, 36]).

Although there was a considerable variability of the kinetic features of the Ca^{2+} concentration changes in the present experiments, the individual transients could be classified as rapid and slow. Regarding rapid transients, their action potential-related character was demonstrated — a finding that is very similar to those reported on neocortical and hippocampal slices [14, 34]. Since the neuronal origin of the rapid Ca^{2+} transients demonstrated in the present work was unambiguously established, their modifications may be regarded as changes reflecting altered neuronal activity. The slow calcium transients, on the other hand, were most likely produced by glial cells [24].

After confirming the action potential-coupled nature of the rapid Ca^{2+} transients, the present work aimed at the reliable detection and correct identification of large numbers of the transients, along with a detailed analysis of their kinetic features. The methodological improvements reported here ensured objective description of the effects of cholinergic stimulation on the Ca^{2+} transients produced by the granule cells of the DCN. A similar approach was chosen by some earlier articles. For example, the usefulness of a similar method for pharmacological screening has already been pointed out (e.g., [16, 37]), and the separation of rapid and slow Ca^{2+} transients was also repeatedly described (e.g., [15, 28, 34]). Among the various approaches, the wavelet

analysis method was utilised for analysing Ca^{2+} oscillations recorded during imaging experiments in neurones [12] and glial cells [29]. In our hands, the wavelet analysis was appropriate for the elimination of the high-frequency noise but adequate detection of the rapid transients required manual control, as the fully automatic method tended to misshape — and occasionally misinterpret — partially fused transients that necessarily accompany high-frequency neuronal activity [14, 34]. The manual control ensured proper identification of solitary rapid transients but could not correct the problem of the fused transients that were, consequently, excluded from the present analysis. This fact resulted in a considerable underestimation of the frequency of the transients at firing rates higher than approx. 10 min^{-1}. Nevertheless, the method was appropriate for demonstrating CCh-induced increases in the frequency of the rapid Ca^{2+} transients — even if exact quantification could not be achieved.

Muscarinic modulation of DCN granule cells

Among the various cell types of the DCN that may generate rapid Ca^{2+} transients, the present study focused on the granule neurones. There were several reasons behind this decision.

First, little is known about the functional properties of these cells, and although there were successful electrophysiological recordings on them (see e.g., [30]), their detailed investigation would require additional approaches.

Second, these neurones could be easily identified on the basis of their size and localisation, without having the danger of misidentification, or needing other methods to support cell classification. In the rat, the somatic diameter of cochlear granule cells is 6–8 μm [1, 22, 23, 30], thus they are the smallest neurones in this nucleus. Because the selection protocol applied in the present work relied on choosing ROIs whose size was the same as the somatic dimensions of the granule cells, it was ensured that only this cell type was considered for data analysis — especially as the Golgi cells (whose size is the closest to that of the granule neurones [22]) hyperpolarize when subjected to cholinergic stimulation [17]. These considerations suggest that our cell selection procedure ensured unambiguous cell identification.

Third, one of our earlier works has shown that electrical stimulation of the giant neurones from the superficial region of the DCN evoked excitatory postsynaptic currents (EPSCs) that were subjected to presynaptic muscarinergic modulation [26]. Considering the structure of the DCN as well as the configuration of this stimulation, the EPSCs were the consequences of the stimulation of the parallel fibres. It was an

obvious question, therefore, whether granule cells themselves are subjected to cholinergic modulation.

The experiments presented here indicate that extracellular application of CCh increases the activity of granule cells directly. However, some of the granule cells generated spontaneous, rapid Ca^{2+} transients even without cholinergic (or any other) stimulation. Although the method applied in the present work did not allow an estimation of the proportion of these spontaneously active granule cells, this finding is in accordance with earlier current-clamp studies [30]. The bulk application of the cholinergic agonist did not allow us to determine whether only synaptic receptors were activated. Nevertheless, the fact that relatively low concentrations of the CCh were also effective suggests that extrasynaptic receptors may have significance in mediating cholinergic actions onto the granule cells.

As for the mechanism of the Ca^{2+} transients, the decisive role of muscarinic acetylcholine receptors is indicated by the strong blocking effect of atropine documented in the present experiments as well as in earlier publications [5, 6, 18]. Depending on the actual subtype, muscarinic receptor activation may cause Ca^{2+} release from intracellular stores and/or may evoke depolarisation (e.g., by closing the KCNQ/M-type K^+ channels), which in turn induces action potential firing and consequent Ca^{2+} entry from the extracellular space [7]. Although there were no specific efforts in the present work to identify the exact mechanism underlying the generation of the Ca^{2+} transients recorded from the granule cells, their action potential-coupled character, the contribution of the Ca^{2+} entry, and the decisive involvement of the M3 receptors in the genesis of the rapid Ca^{2+} transients were clearly established.

While the present work focused on the consequences of direct cholinergic stimulation of the granule neurones, it must be noted that under physiological conditions (i.e., when the synaptic transmission is not interfered with), cholinergic activity may stimulate granule cells via an indirect pathway, too. It is known that the Golgi cells of the DCN are inhibitory interneurones that make synaptic contacts with, inter alia, the granule cells [17, 22]. Their muscarinic receptor-induced hyperpolarisation [17], consequently, may result in a dysinhibition phenomenon, resulting in an increased activity of the granule cells (or at least their certain sub-populations).

When comparing the frequencies of the Ca^{2+} transients in the absence and in the presence of hexamethonium, no statistically significant blocking effect was found. This finding is in line with earlier reports showing the presence of the nicotinic acetylcholine receptors in the rat CN without apparent function [13, 43]. The results presented here

also underscore a dominant role of the muscarinic receptors in the cholinergic modulation of the granule neurones.

Granule cells of the DCN receive multimodal inputs from various sources [25, 31], and send information to the pyramidal, giant, and cartwheel neurones via the parallel fibre network. The exact physiological role of this circuitry is not known at present, but widely accepted hypotheses emphasize its similarity to those present in the cerebellum. Based on various analogies, it can be postulated that the granule cell – parallel fibre pathway may play some roles in the reconciliation of the primary auditory and related somatosensory information (for a comprehensive review see [25]).

The most intriguing question to be answered, however, is the precise role of cholinergic modulation in the function of the DCN. Several data obtained under various experimental conditions point toward a facilitatory influence of cholinergic innervation at different stages of the auditory pathway. In the CN, for example, possible cholinergic excitation of the ventral part was proposed [2]; an amplifier function of cholinergic modulation in the DCN was hypothesized [18], and most recently an increased activity of the giant cells on CCh application has been reported [26]. The latter effect might be (at least partly) the consequence of the elimination of the short-term depression present at the parallel fibre-giant cell synapses. Since cholinergic activity simultaneously increases the firing activity of the granule cells, the cholinergic stimulation may contribute to shifting the plasticity of these synapses towards long-term potentiation, similarly to that shown in the cases of the parallel fiber-pyramidal neurone synapses [9]. An important argument supporting this idea is that mainly M3 receptors mediate the cholinergic modulation of both the excitatory postsynaptic potentials at the parallel fiber-giant cell synapses and the activity of the granule neurones. Although the present findings emphasize the important modulatory roles of cholinergic inputs in the function of the DCN and shed light on some of the possible mechanisms of these modulatory effects, further experiments are needed to explore the exact functional and molecular details of this mechanism. These future efforts should reveal the factors contributing to the genesis of the rapid Ca^{2+} transients and should provide analysis of the roles of the individual muscarinic receptor subtypes using more specific antagonists.

Acknowledgements

This work was supported by a grant from the Hungarian Scientific Research Fund (OTKA K-72812), by an NHMRC (National Health & Medical Research Council) Australia Fellowship Grant awarded to Dr George Paxinos (Grant #568605), and by the Australian Research Council Thinking Systems Initiative (TS0669860).

Ethical considerations

The protocols used in the animal experiment were approved by the Committee of Animal Research of the University of Debrecen and by the Animal Care and Ethics Committee of The University of New South Wales, and they were in accordance with the relevant national and institutional guidelines on the care of research animals.

Conflict of interest

The authors declare that they have no conflict of interest.

References

1. Balakrishnan V, Trussell LO (2008) Synaptic inputs to granule cells of the dorsal cochlear nucleus. J Neurophysiol 99:208-219.
2. Bledsoe SCJ, Koehler S, Tucci DL, Zhou J, Le Prell CG, Shore SE (2009) Ventral cochlear nucleus responses to contralateral sound are mediated by CN-commissural and olivocochlear pathways. J Neurophysiol 102:886-900.
3. Bon-Jego M, Yuste R (2007) Persistently active, pacemaker-like neurons in neocortex. Front Neurosci 1:123-129.
4. Brown MC, Liberman MC, Benson TE, Ryugo DK (1988) Brainstem branches from olivocochlear axons in cats and rodents. J Comp Neurol 278:591-603.
5. Chen K, Waller HJ, Godfrey DA (1994) Cholinergic modulation of spontaneous activity in rat dorsal cochlear nucleus. Hear Res 77:168-176.
6. Chen K, Waller HJ, Godfrey DA (1995) Muscarinic receptor subtypes in rat dorsal cochlear nucleus. Hear Res 89:137-145.
7 . Delmas P, Brown DA (2005) Pathways modulating neural KCNQ/M (Kv7) potassium channels. Nat Rev Neurosci 6:850-862.
8. Felder CC (1995) Muscarinic acetylcholine receptors: signal transduction through multiple effectors. The FASEB Journal 9:619-625.
9. Fujino K, Oertel D (2003) Bidirectional synaptic plasticity in the cerebellum-like mammalian dorsal cochlear nucleus. Proc Natl Acad Sci USA 100:265-270.
10. Garaschuk O, Milos RI, Grienberger C, Marandi N, Adelsberger H, Konnerth A (2006) Optical monitoring of brain function in vivo: from neurons to networks. Pflügers Arch 453:385-396.
11. Godfrey DA, Park-Hellendall JL, Dunn JD, Ross CD (1987) Effects of trapezoid body and superior olive lesions on choline acetyltransferase activity in the rat cochlear nucleus. Hear Res 28: 253-270.
12. Gorbunova YV, Spitzer NC (2002) Dynamic interactions of cyclic AMP transients and spontaneous Ca^{2+} spikes. Nature 418:93-96.
13. Happe HK, Morley BJ (1998) Nicotinic acetylcholine receptors in rat cochlear nucleus: [125I]-alpha-bungarotoxin receptor autoradiography and in situ hybridization of alpha 7 nAChR subunit mRNA. J Comp Neurol 397:163-180.
14. Helmchen F, Imoto K, Sakmann B (1996) Ca^{2+} buffering and action potential-evoked Ca^{2+} signaling in dendrites of pyramidal neurons. Biophys J 70:1069-1081.

15. Ikegaya Y, Bon-Jego M, Yuste R (2005) Large-scale imaging of cortical network activity with calcium indicators. Neurosci Res 52:132-138.
16. Ikegaya Y (2008) Large-scale Recordings for Drug Screening in Neural Circuit Systems. Yakugaku Zasshi 128:1251-1257.
17. Irie T, Fukui I, Ohmori H (2006) Activation of GIRK channels by muscarinic receptors and group II metabotropic glutamate receptors suppresses Golgi cell activity in the cochlear nucleus of mice. J Neurophysiol 96:2633-2644.
18. Jin YM, Godfrey DA (2006) Effects of cochlear ablation on muscarinic acetylcholine receptor binding in the rat cochlear nucleus. J Neurosci Res 83:157-166.
19. Kane EC (1974) Synaptic organisation in the dorsal cochlear nucleus of the cat: a light and electron microscopic study. J Comp Neurol 155:301-330.
20. McDonald DM , Rasmussen GL (1971) Ultrastructural characteristics of synaptic endings in the cochlear nucleus having acetylcholinesterase activity. Brain Res 28:1-18.
21. Mellott JG, Motts SD, Schofield BR (2011) Multiple origins of cholinergic innervation of the cochlear nucleus. Neuroscience 180:138-147.
22. Mugnaini E, Osen KK, Dahl AL, Friedrich VL, Korte G (1980a) Fine structure of granule cells and related interneurons (termed Golgi cells) in the cochlear nuclear complex of cat, rat and mouse. J Neurocytol 9:537-570.
23. Mugnaini E, Warr WB, Osen KK (1980b) Distribution and light microscopic features of granule cells in the cochlear nuclei of cat, rat, and mouse. J Comp Neurol 191:581-606.
24. Nimmerjahn A, Kirchhoff F, Kerr JND, Helmchen F (2004) Sulforhodamine 101 as a specific marker of astroglia in the neocortex in vivo. Nat Meth 1:31-37.
25. Oertel D, Young ED (2004) What's a cerebellar circuit doing in the auditory system? Trends Neurosci 27:104-110.
26. Pál B, Kőszeghy Á, Pap P, Bakondi G, Pocsai K, Szücs G, Rusznák Z (2009) Targets, receptors and effects of muscarinic neuromodulation on giant neurones of the rat dorsal cochlear nucleus. Eur J Neurosci 30:769-782.
27. Pap P, Kőszeghy Á, Szücs G, Rusznák Z (2009) Cytoplasmic Ca^{2+} concentration changes evoked by cholinergic stimulation in primary astrocyte cultures prepared from the rat cochlear nucleus. Hear Res 255:73-83.

28. Peterlin ZA, Kozloski J, Mao BQ, Tsiola A, Yuste R (2000) Optical probing of neuronal circuits with calcium indicators. Proc Natl Acad Sci US America 97:3619-3624.
29. Ruffinatti FA, Lovisolo D, Distasi C, Ariano P, Erriquez J, Ferraro M (2011) Calcium signals: Analysis in time and frequency domains. J Neurosci Meth 199:310-320.
30. Rusznák Z, Forsythe ID, Brew HM, Stanfield PR (1997) Membrane currents influencing action potential latency in granule neurons of the rat cochlear nucleus. Eur J Neurosci 9:2348-2358.
31. Ryugo DK, Haenggeli CA, Doucet JR (2003) Multimodal inputs to the granule cell domain of the cochlear nucleus. Exp Brain Res 153:477-485.
32. Schwartz TH, Rabinowitz D, Unni V, Kumar VS, Smetters DK, Tsiola A, Yuste R (1998) Networks of coactive neurons in developing layer 1. Neuron 20:541-552.
33. Sherriff FE , Henderson Z (1994) Cholinergic neurons in the ventral trapezoid nucleus project to the cochlear nuclei in the rat. Neuroscience 58:627-633.
34. Smetters D, Majewska A, Yuste R (1999) Detecting action potentials in neuronal populations with calcium imaging. Methods 18:215-221.
35. Szabó LZ, Vincze J, Csernoch L, Szentesi P (2010) Improved spark and ember detection using stationary wavelet transforms. J Theor Biol 264:1279-1292.
36. Takahashi N, Sasaki T, Usami A, Matsuki N, Ikegaya Y (2007) Watching neuronal circuit dynamics through functional multineuron calcium imaging (fMCI). Neurosci Res 58:219-225.
37. Usami A, Sasaki T, Satoh N, Akiba T, Yokoshima S, Fukuyama T, Yamatsugu K, Kanai M, Shibasaki M, Matsuki N, Ikegaya Y (2008) Oseltamivir Enhances Hippocampal Network Synchronization. J Pharmacol Sci 106:659-662.
38. Wegner F, Both M, Fink R (2011) Automated detection of elementary calcium release events using the á trous wavelet transform. Biophys J 90:2151-2163.
39. Widrow B, Lehr MA (1990) 30 years of adaptive neural networks: perception, madaline, and backpropagation. Proc IEEE 78:1415-1442.
40. Wright DD , Ryugo DK (1996) Mossy fiber projections from the cuneate nucleus to the cochlear nucleus in the rat. J Comp Neurol 365:159-172.
41. Yao W, Godfrey DA (1995) Immunohistochemistry of muscarinic acetylcholine receptors in rat cochlear nucleus. Hear Res 89:76-85.

42. Yao W, Godfrey DA, Levey AI (1996) Immunolocalization of muscarinic acetylcholine subtype 2 receptors in rat cochlear nucleus. J Comp Neurol 373:27-40.
43. Yao W, Godfrey DA (1999) Vesicular acetylcholine transporter in the rat cochlear nucleus: An immunohistochemical study. J Histochem Cytochem 47:83-90.
44. Zhang JS, Kaltenbach JA (2000) Modulation of spontaneous activity by acetylcholine receptors in the rat dorsal cochlear nucleus in vivo . Hear Res 140:7-17.

Supplementary material

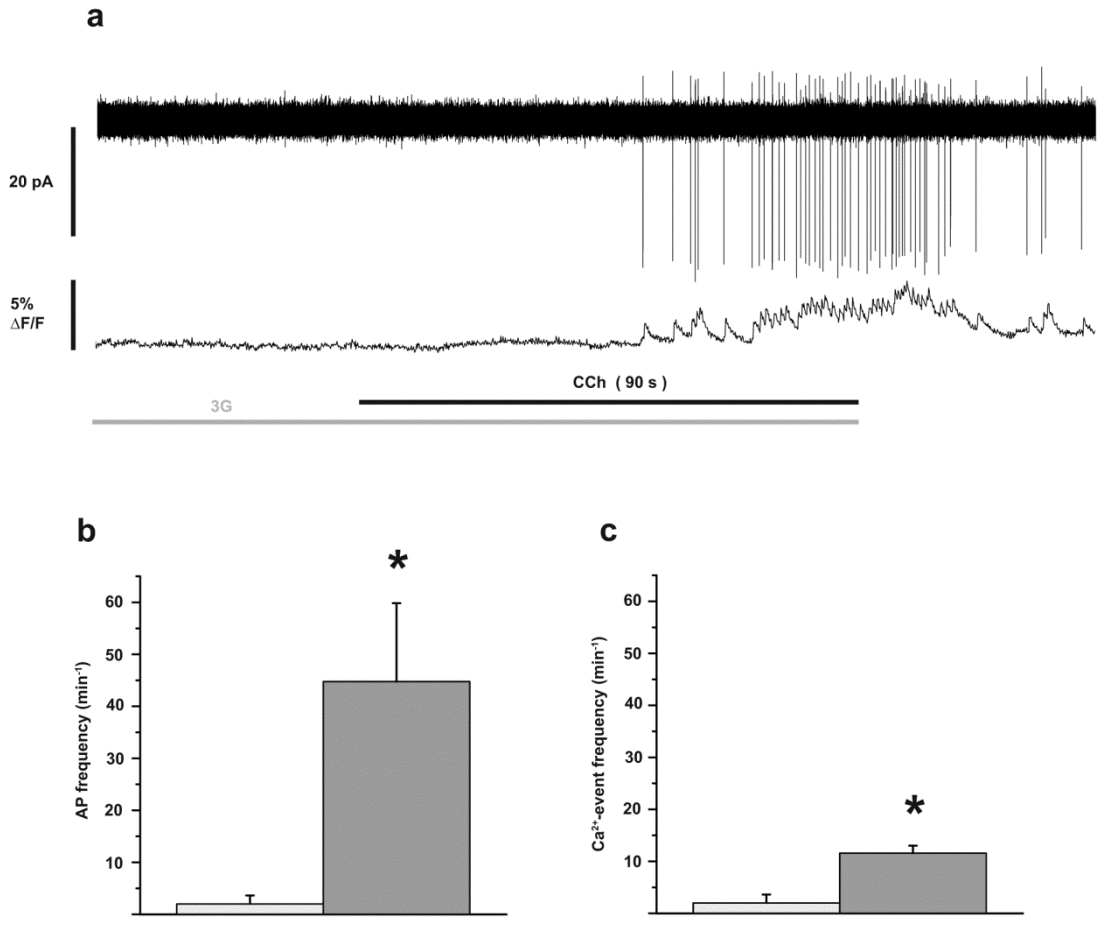

Supplementary Figure 1: Effects of CCh on the action potential firing of granule neurones. **Panel a**: simultaneous current (upper trace) and fluorescence (lower trace) recording from a granule cell in 3G cocktail and in the presence of 100 µM CCh (the incubation times are indicated by horizontal lines). **Panels b–c:** synopsis of the data obtained in experiments carried out as indicated in panel a (n = 6). Light grey columns indicate the control frequency of the action potentials (panel b) and the rapid transients (panel c) measured in 3G cocktail. 100 µM CCh (dark grey columns) increased the frequency of both the action potentials (panel b) and the rapid Ca^{2+} transients (panel c). *: $p < 0.05$.

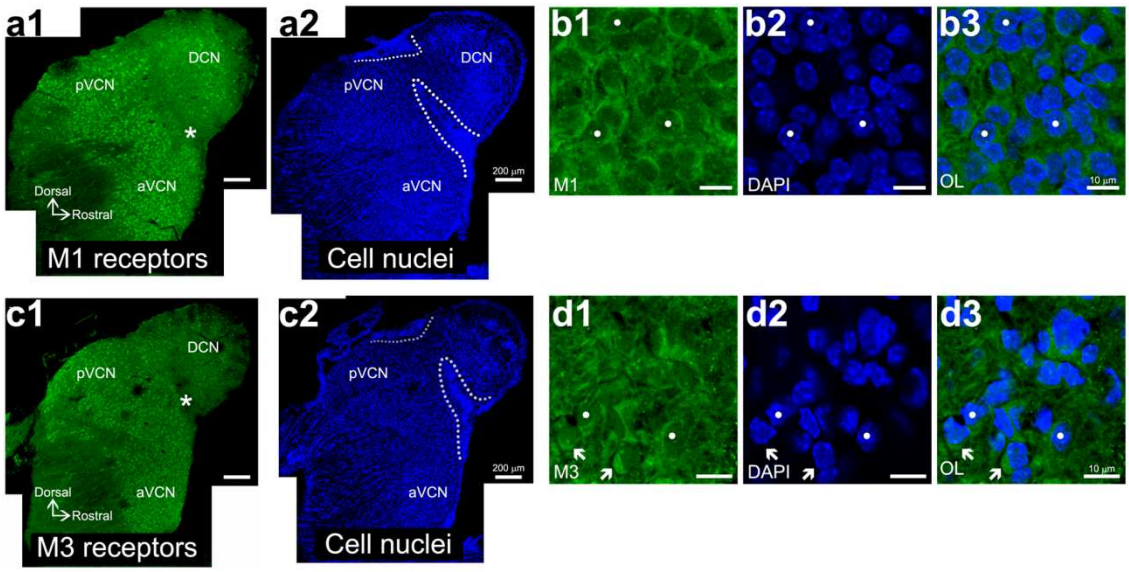

Supplementary Figure 2: M1 and M3 receptor-specific immunolabelling in the cochlear nucleus of a 15-day-old rat. **Panels a1–a2**: composite images demonstrating a low magnification overview of the M1 receptor-specific immunolabelling pattern (a1) and the distribution of the cell nuclei (a2). In a1, asterisk marks part of the granule cell region from where the high magnification images (b1–b3) were taken. In a2, the visible parts of the granule cell layer separating the dorsal and ventral cochlear nuclei are marked with dotted lines. DCN, aVCN, and pVCN stand for dorsal cochlear nucleus, antero-ventral cochlear nucleus, and postero-ventral cochlear nucleus, respectively. **Panels b1–b3**: high magnification images depicting the M1-specific labelling pattern of granule cells. b1: M1-specific immunopositivity (green), b2: DAPI labeling (blue), b3: overlay image. White dots mark some of the granule cells demonstrating strong M1-specific immunopositivites. **Panels c1–c2**: composite image demonstrating a low magnification overview of the M3 receptor-specific immunolabelling pattern (c1) and the distribution of the cell nuclei (c2). The meanings of the letters and special markings are the same as in a1–a2. **Panels d1–d3**: high magnification images depicting some examples of M3 positive granule cells. d1: M3-specific immunopositivity, d2: DAPI labelling, d3: overlay image. White dots mark some of the granule cells demonstrating strong M3-specific immunopositivities. In the cases of the cells marked with arrows, the immunopositivity pattern may correspond to receptor aggregation on the cell surface.